


# Na<sub>X</sub> Channel Is a Physiological [Na<sup>+</sup>] Detector in Oxytocin- and Vasopressin-Releasing Magnocellular Neurosecretory Cells of the Rat Supraoptic Nucleus

Sandra Salgado-Mozo,<sup>1,2</sup>  Zahra S. Thirouin,<sup>1</sup> Joshua C. Wyrosdic,<sup>1</sup> Ubaldo García-Hernández,<sup>2</sup> and Charles W. Bourque<sup>1</sup>

<sup>1</sup>Brain Repair and Integrative Neuroscience Program, Research Institute of McGill University Health Center, Montréal, Québec H3G1A4, Canada and <sup>2</sup>Department of Physiology, Biophysics and Neurosciences, Centre for Research and Advanced Studies, Instituto Politécnico Nacional, 07360 Mexico City, Mexico

The *Scn7A* gene encodes Na<sub>X</sub>, an atypical noninactivating Na<sup>+</sup> channel, whose expression in sensory circumventricular organs is essential to maintain homeostatic responses for body fluid balance. However, Na<sub>X</sub> has also been detected in homeostatic effector neurons, such as vasopressin (VP)-releasing magnocellular neurosecretory cells (MNC<sup>VP</sup>) that secrete VP (antidiuretic hormone) into the bloodstream in response to hypertonicity and hypernatremia. Yet, the physiological relevance of Na<sub>X</sub> expression in these effector cells remains unclear. Here, we show that rat MNC<sup>VP</sup> in males and females is depolarized and excited in proportion with isosmotic increases in [Na<sup>+</sup>]. These responses were caused by an inward current resulting from a cell-autonomous increase in Na<sup>+</sup> conductance. The Na<sup>+</sup>-evoked current was unaffected by blockers of other Na<sup>+</sup>-permeable ion channels but was significantly reduced by shRNA-mediated knockdown of *Scn7A* expression. Furthermore, reducing the density of Na<sub>X</sub> channels selectively impaired the activation of MNC<sup>VP</sup> by systemic hypernatremia without affecting their responsiveness to hypertonicity *in vivo*. These results identify Na<sub>X</sub> as a physiological Na<sup>+</sup> sensor, whose expression in MNC<sup>VP</sup> contributes to the generation of homeostatic responses to hypernatremia.

**Key words:** electrophysiology; Na<sub>X</sub> channel; osmoregulation; sodium detection; supraoptic nucleus; vasopressin

## Significance Statement

In this study, we provide the first direct evidence showing that the sodium-sensing channel encoded by the *Scn7A* gene (Na<sub>X</sub>) mediates cell-autonomous sodium detection by MNCs in the low millimolar range and that selectively reducing the expression of these channels in MNCs impairs their activation in response to a physiologically relevant sodium stimulus *in vitro* and *in vivo*. These data reveal that Na<sub>X</sub> operates as a sodium sensor in these cells and that the endogenous sensory properties of osmoregulatory effector neurons contribute to their homeostatic activation *in vivo*.

## Introduction

Systemic osmoregulation is the vital process by which total extracellular solute concentration (osmolality) is maintained within the physiological range. Sodium (Na<sup>+</sup>) is the dominant

extracellular cation, and its concentration varies in parallel with extracellular osmolality under most conditions. Regulating the concentration of extracellular Na<sup>+</sup> ([Na<sup>+</sup>]<sub>o</sub>) is therefore an important component of osmoregulation. Indeed, the effector mechanisms involved in this process include controlling the intake of water and Na<sup>+</sup> as well as the release of hormones that regulate Na<sup>+</sup> and water excretion by the kidney (Denton et al., 1996; Bourque, 2008; Zimmerman et al., 2017; Gizowski and Bourque, 2018). Previous studies have identified neurons and brain pathways that form specific components of the osmoregulatory network. For example, oxytocin (OT)-releasing magnocellular neurosecretory cells (MNC<sup>OT</sup>) and vasopressin (VP)-releasing magnocellular neurosecretory cells (MNC<sup>VP</sup>) in the supraoptic (SON) and paraventricular nuclei are effector neurons that respectively command natriuresis (Huang et al., 1995) and antidiuresis (Robertson et al., 1976). An essential requirement

Received June 29, 2023; revised Sep. 8, 2023; accepted Sep. 25, 2023.

Author contributions: S.S.-M., U.G.-H., and C.W.B. designed research; S.S.-M., Z.S.T., and J.C.W. performed research; S.S.-M. and J.C.W. analyzed data; S.S.-M. and C.W.B. wrote the paper.

This work was supported by Canadian Institutes of Health Research Grant FDN 143337, Centro de Investigación y de Estudios Avanzados (CINVESTAV) Grant 501100008688 (U.G.-H.), a grant from the Canada Foundation for Innovation and a James McGill Chair (C.W.B.), Consejo Nacional de Ciencia y Tecnología (CONACYT) Studentship (S.S.-M.), McGill University Healthy Brains for Healthy Lives Program Studentship (J.C.W.), and Fonds de Recherche Québec Santé.

The authors declare no competing financial interests.

Correspondence should be addressed to Charles W. Bourque at charles.bourque@mcgill.ca.

<https://doi.org/10.1523/JNEUROSCI.1203-23.2023>

Copyright © 2023 the authors

for osmoregulation is that effector neurons receive sensory information regarding the ongoing state of hydration of the body (i.e., feedback signals; Bourque, 2008) as well as predictive signals that anticipate challenges (i.e., feedforward signals; Zimmerman et al., 2017; Kim et al., 2021). Indeed, previous studies have shown that sensory feedback signals are generated by osmo- and  $\text{Na}^+$ -sensitive neurons in the subfornical organ (SFO) and organum vasculosum lamina terminalis (OVLT; Olsson and Kolmodin, 1974; Andersson, 1977; McKinley et al., 1978; Vivas et al., 1990; Anderson et al., 2000; Ciura et al., 2011; Oka et al., 2015; Augustine et al., 2018; Ciura et al., 2018; Nomura et al., 2019; Pool et al., 2020), and that afferent signals from the gastrointestinal tract provide feedforward information about ingested fluids (Mandelblat-Cerf et al., 2017; Augustine et al., 2018; Zimmerman et al., 2019; Kim et al., 2021). Surprisingly, *in vitro* work has shown that effector neurons such as  $\text{MNC}^{\text{VP}}$  and  $\text{MNC}^{\text{OT}}$  are intrinsically osmosensitive (Mason, 1980; Abe and Ogata, 1982; Oliet and Bourque, 1993; Prager-Khoutorsky et al., 2014) and  $\text{Na}^+$  sensitive (Voisin et al., 1999). However, the effects of selectively ablating these properties in effector neurons have not been examined. Therefore, it is unknown if these intrinsic properties add significantly to signals received from feedback and feedforward sensors to command optimal homeostatic responses during physiological stimulation *in vivo*.

Our understanding of mechanisms responsible for  $\text{Na}^+$  detection by  $\text{MNC}^{\text{VP}}$  and  $\text{MNC}^{\text{OT}}$  remains incomplete (Voisin and Bourque, 2002; Noda and Matsuda, 2022). In principle, these neurons could detect rises in  $[\text{Na}^+]_o$  through the depolarizing effect of an inward current caused by increasing the driving force across  $\text{Na}^+$ -permeable leak channels. Such an effect could be mediated through leak channels such as epithelial  $\text{Na}^+$  channels (ENaCs; Teruyama et al., 2012), nonselective cation channels such as the transient receptor potential vanilloid type 1 (Trpv1; Voisin et al., 1999) or noninactivating voltage-gated  $\text{Na}^+$  channels (VGSCs; Black et al., 2014). Although  $\text{MNC}^{\text{VP}}$  and  $\text{MNC}^{\text{OT}}$  express all three subunits ( $\alpha$ ,  $\beta$ ,  $\gamma$ ) of ENaCs (Teruyama et al., 2012; Sharma et al., 2017), a variety of VGSCs (Waxman et al., 2000; Black et al., 2014) and variants of Trpv1 (Sharif-Naeini et al., 2006; Zaelzer et al., 2015), it remains unclear if such channels mediate neuronal excitation in response to a physiological increase in  $[\text{Na}^+]_o$  in euhydrated animals. By contrast, experiments on the OVLT and SFO have shown that  $[\text{Na}^+]$  detection can be mediated by the atypical  $\text{Na}^+$  channel  $\text{Na}_x$ , which is encoded by the *Scn7A* gene (Hiyama et al., 2004; Shimizu et al., 2007; Hiyama et al., 2010; Noda and Hiyama, 2015; Nomura et al., 2019). Although  $\text{Na}_x$  has been reported to be expressed in the rat SON (Nehmé et al., 2012), the potential role of these channels for functional  $\text{Na}^+$  detection by  $\text{MNC}^{\text{VP}}$  and  $\text{MNC}^{\text{OT}}$  has not been investigated. In this study we show  $\text{Na}_x$  channels enable  $\text{Na}^+$  detection by  $\text{MNC}^{\text{VP}}$  and  $\text{MNC}^{\text{OT}}$  *in vitro* and contribute to the activation of these neurons by a physiologically relevant hypernatremic stimulus *in vivo*.

## Materials and Methods

**Drugs and antibodies.** All drugs were kept in stocks. Tetrodotoxin (TTX) citrate, 10 mM (in water, Alomone Labs); SB-366791, 17.3 mM (in DMSO; Sigma-Aldrich); and benzamil hydrochloride hydrate, 5.6 mM (in water; Sigma-Aldrich). Antibodies from commercial sources are anti-SCN7A polyclonal antibody (1:200; catalog #bs-12127R, Bioss Antibodies), anti-vasopressin antibody (1:1000; catalog #403004, SYSY), anti-oxytocin antibody, clone 4G11 (1:1000; MilliporeSigma), anti-c-fos

rabbit monoclonal (1:2000; catalog #226 008, SYSY), and anti-GFAP antibody (1:500; Abcam).

**Animals.** Adult female and male Wistar rats were used in this study. Rats were maintained on a 12:12 h light/dark cycle and provided with *ad libitum* access to food and water. All procedures involving animals were conducted in accord with protocols approved by the Facility Animal Care Committee of McGill University and Unidad de Producción y Experimentación de Animales de Laboratorio–Centro de Investigación y de Estudios Avanzados (CINVESTAV) according to the norm-062-ZOO-1999. Experiments at McGill University were performed on transgenic female and male Wistar rats (12–24 weeks) that express green fluorescent protein (GFP) and red fluorescent protein (RFP) under the control of the *Avp* gene and *Oxt* gene promoter, respectively. Experiments at CINVESTAV were performed on adult male Wistar rats (5–8 weeks).

**Acute slice preparation.** Acute hypothalamic slices 400  $\mu\text{m}$  thick were cut using a VT-1200 vibratome (Leica Biosystems) at an angle of  $38^\circ$  relative to the surface of the cortex and submerged in warm oxygenated (95%  $\text{O}_2$ , 5%  $\text{CO}_2$ ;  $31^\circ\text{C}$ ) artificial CSF (ACSF) for at least 1 h before recordings began (Stachniak et al., 2014). The ACSF contained the following (in mM): 120 NaCl, 3 KCl, 1.23  $\text{NaH}_2\text{PO}_4$ , 1.48  $\text{MgCl}_2$ , 2  $\text{CaCl}_2$ , 26  $\text{NaHCO}_3$ , and 10 glucose, osmolality  $295 \pm 3$  mOsm/kg.

**Ramp-like  $[\text{Na}^+]_o$  stimulation in slices.** Following  $>3$  min baseline,  $\text{Na}^+$  stimuli in slices were delivered as ramp-like increases (3 min) and decreases ( $\sim 6$  min) in  $[\text{Na}^+]_o$ . Peak concentrations achieved during these tests were +3, +4, +9, and +15 mM  $[\text{Na}^+]_o$  determined by electrolyte analysis. These ramps were achieved by the infusion of more concentrated solutions (+4, +8, +15, +36 mM  $[\text{Na}^+]_o$ ; 2 ml/min) into a recording chamber featuring a static volume of 3.5 ml. The +4 mM  $[\text{Na}^+]_o$  hypernatremic isosmotic ACSF contained the following (in mM): 110 NaCl, 7  $\text{Na}_2\text{SO}_4$ , 3 KCl, 1.23  $\text{NaH}_2\text{PO}_4$ , 1.48  $\text{MgCl}_2$ , 2  $\text{CaCl}_2$ , 26  $\text{NaHCO}_3$ , and 10 glucose, osmolality  $295 \pm 3$  mOsm/kg. The +8 mM  $[\text{Na}^+]_o$  hypernatremic isosmotic ACSF contained the following (in mM): 100 NaCl, 14  $\text{Na}_2\text{SO}_4$ , 3 KCl, 1.23  $\text{NaH}_2\text{PO}_4$ , 1.48  $\text{MgCl}_2$ , 2  $\text{CaCl}_2$ , 26  $\text{NaHCO}_3$ , and 10 glucose, osmolality  $295 \pm 3$  mOsm/kg. The +15 mM  $[\text{Na}^+]_o$  hypernatremic isosmotic ACSF contained the following (in mM): 75 NaCl, 35  $\text{Na}_2\text{SO}_4$ , 3 KCl, 1.23  $\text{NaH}_2\text{PO}_4$ , 1.48  $\text{MgCl}_2$ , 2  $\text{CaCl}_2$ , 26  $\text{NaHCO}_3$ , and 10 glucose, osmolality  $298 \pm 3$  mOsm/kg. The +36 mM  $[\text{Na}^+]_o$  hypernatremic isosmotic ACSF contained the following (in mM): 78  $\text{Na}_2\text{SO}_4$ , 3 KCl, 1.23  $\text{NaH}_2\text{PO}_4$ , 1.48  $\text{MgCl}_2$ , 2  $\text{CaCl}_2$ , 26  $\text{NaHCO}_3$ , and 10 glucose, osmolality  $295 \pm 3$  mOsm/kg.

**Electrophysiological recordings in slices.** Voltage- and current-clamp recordings were obtained using whole-cell configuration from identified  $\text{MNC}^{\text{VP}}$  and  $\text{MNC}^{\text{OT}}$ . In all the experiments, an agar bridge of NaCl (1 M) was used to eliminate voltage offsets at the ground electrode. Voltage-clamp recordings were performed with a holding voltage of  $-50$  mV. Patch pipettes were prepared from glass capillary tubes filled with a solution containing the following (in mM): 120 K-glucuronate, 10 HEPES, 1  $\text{MgCl}_2$ , 0.1  $\text{CaCl}_2$ , 10 KCl, 1 EGTA- $\text{Na}_4$ , 2  $\text{Na}_2\text{ATP}$ , and 1  $\text{NaGTP}$ ,  $285 \pm 3$  mOsm/kg, pH 7.40. Pipette resistance in the bath was 3–5 M $\Omega$ . To determine  $\text{Na}^+$  sensitivity in slice experiments involving +15 mM  $\text{Na}^+$  stimulation (Fig. 1H), values were measured at  $t = 0$  (baseline),  $t = 1$ ,  $t = 2$ , and  $t = 3$  min (average of 2 s) and plotted as a function of chamber  $[\text{Na}^+]_o$  at each time point and fitted by a linear regression. For measurement of peak responses, data averaged at  $t = 2.75$ – $3.0$  min were compared with baseline (average of data collected 15 s before  $t = 0$ ). In spiking cells, membrane potential was determined as the peak voltage observed in an all-points histogram constructed from data segments that included occasional silent intervals. Some recordings were obtained in the presence of TTX 0.5  $\mu\text{M}$ , benzamil 2  $\mu\text{M}$ , or SB-366791 3  $\mu\text{M}$ . Signals were recorded using a MultiClamp 700B amplifier, digitized by a DigiData 1440A digitizer (Molecular Devices) at 10 kHz and filtered at 2 kHz. Electrophysiological data were analyzed using pClamp software (Molecular Devices).

**Isolated cell preparation and solutions.** Wistar rats were killed by decapitation, and the brain was rapidly removed and placed in Locke's buffer containing the following (in mM): 110 NaCl, 5 KCl, 1.2  $\text{KH}_2\text{PO}_4$ , 1.2  $\text{MgSO}_4$ , 1.8  $\text{CaCl}_2$ , 10 glucose, 26  $\text{NaHCO}_3$ , and 10 HEPES,  $290 \pm 5$  mOsm/kg, pH 7.4. The SON was dissected using iridectomy scissors from 1-mm-thick slices, and the tissue block was placed in Locke's buffer

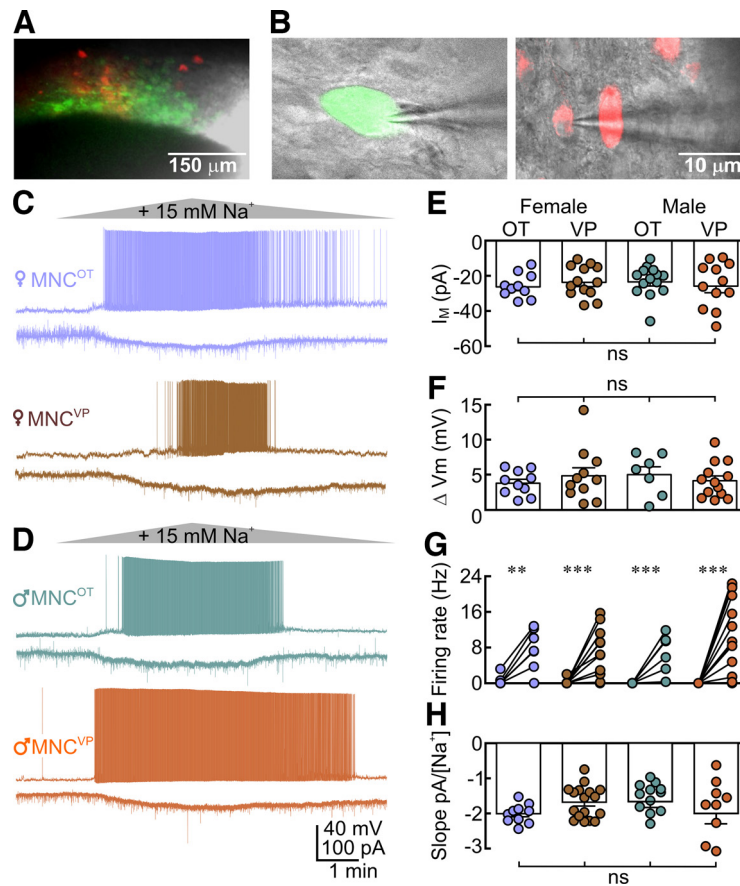


**Figure 1.** Effects of high  $[\text{Na}^+]$  on  $\text{MNC}^{\text{OT}}$  and  $\text{MNC}^{\text{VP}}$  of female and male rats. **A**, Low-power ( $10\times$ ) view of the SON in a live horizontal hypothalamic slice from a transgenic rat in which RFP is expressed in  $\text{MNC}^{\text{OT}}$ , and GFP is expressed in  $\text{MNC}^{\text{VP}}$ . Bottom, The dark structure is the optic tract. **B**, High-power ( $60\times$ ) views of  $\text{MNC}^{\text{VP}}$  (left) and  $\text{MNC}^{\text{OT}}$  (right) targeted by patch electrodes. **C**, Effects of increasing extracellular  $[\text{Na}^+]$  by 15 mM while maintaining osmolality constant (gray ramp; see above, Materials and Methods) on  $\text{MNC}^{\text{OT}}$  (lilac) and  $\text{MNC}^{\text{VP}}$  (brown) in slices from female rats. Top traces show voltage effects of the stimulus in current clamp, bottom traces show effects of the stimulus on membrane current (voltage clamp). **D**, Effects of increasing  $[\text{Na}^+]$  on  $\text{MNC}^{\text{OT}}$  (teal) and  $\text{MNC}^{\text{VP}}$  (orange) in slices from male rats (layout the same as in **C**). To quantify these traces, we compared values observed at the end of the stimulus with baseline values before stimulus onset (see above, Materials and Methods). **E**, Bar graphs show mean  $\pm$  SEM amplitudes of the  $\text{Na}^+$ -induced current ( $I_m$ ) in all conditions (Each circle indicates data from a different cell.). ns, Not significant. **F**, Bar graphs show mean  $\pm$  SEM amplitudes of the  $\text{Na}^+$ -induced depolarization ( $\Delta V_m$ ) in all conditions (Each circle indicates data from a different cell.). **G**, Two-point plots show changes in firing rate induced by the  $\text{Na}^+$  stimulus in all conditions. Each line joins control (left) and stimulated firing rates (right) from individual cells; \*\*\* $p < 0.001$ . **H**, Bar graphs show mean  $\pm$  SEM  $\text{Na}^+$  sensitivity of all subtypes of MNCs expressed as the slope of linear regressions fitted through data plotting  $I_m$  as a function of  $[\text{Na}^+]_o$  for each cell.

containing 1.5 mg/ml of papain (Sigma-Aldrich) for 30 min at  $37^\circ\text{C}$ . The tissue was then transferred to papain-free Locke's buffer and triturated using fire-polished Pasteur pipettes and centrifuged at 1000 rpm for 2 min. The supernatant was discarded, and the concentrated cells were resuspended in 500  $\mu\text{l}$  of neurobasal-A medium containing B37 serum (Thermo Fisher Scientific). MNCs were plated on glass-bottomed recording chambers coated with type-1 collagen (0.01%; Sigma-Aldrich). Only cells with a diameter  $>20\mu\text{m}$  were recorded, and previous work has shown that such cells are MNCs (Oliet and Bourque, 1992).

**Electrophysiology in isolated cells.** For current–voltage ( $I$ – $V$ ) analysis, voltage-clamp recordings in whole-cell mode were performed with a holding voltage of  $-40\text{ mV}$ . The internal solution contained the following (in mM): 60 NaCl, 25 CsCl, 2 KCl, 10 HEPES, 5 TEA-Cl, 4 Mg-ATP, 0.02 EGTA-Na, and 110 mannitol,  $290 \pm 5\text{ mOsmol/kg}$ , pH 7.40. Pipette resistance in the bath was 4–8 M $\Omega$ . In each case a period of 20 s of stable baseline activity was recorded in external solution containing the following (in mM): 60 NaCl, 8.9 CsCl, 2 KCl, 2.4 CaCl<sub>2</sub>, 1.3 MgCl<sub>2</sub>, 0.5 CdCl<sub>2</sub>, 10 HEPES, 10 TEA-Cl, 5 glucose, 1 4-AP, 0.0005 TTX, and 110 mannitol,  $290 \pm 5\text{ mOsmol/kg}$ , pH 7.40. A  $+72\text{ mM}$   $[\text{Na}^+]$  hypernatremic-isosmotic solution was then applied, which contained the following (in mM): 60 NaCl, 24 Na<sub>3</sub>-citrate, 8.9 CsCl, 2 KCl, 2.4 CaCl<sub>2</sub>, 1.3 MgCl<sub>2</sub>, 10 HEPES, 10 mannitol, 5 glucose, 0.5 CdCl<sub>2</sub>, 10 TEA-Cl, 1 4-AP, and 0.0005 TTX,  $290 \pm 5\text{ mOsmol/kg}$ , pH 7.40 (all from Sigma-Aldrich). Voltage ramp protocols ( $-80$  to  $80\text{ mV}$ ) were used to obtained

$I$ – $V$  plots before (control) and 20 s after high ( $+72\text{ mM}$ )  $\text{Na}^+$ . For calculation of mean reversal potential ( $E_{\text{rev}}$ ), values were corrected for a liquid junction error of  $-4.7\text{ mV}$ . Signals were recorded using an Axopatch 200A amplifier, digitized by DigiData 1200 (Molecular Devices) and filtered at 5 kHz. Electrophysiological data were analyzed using pClamp (Molecular Devices).

Voltage and current responses to smaller stimuli ( $+5$  and  $+36\text{ mM}$   $[\text{Na}^+]$ ) were also recorded. In each case a period of 20 s of stable baseline activity was compared with activity recorded in high  $\text{Na}^+$ . For  $+5\text{ mM}$  stimulation, the baseline solution contained the following (in mM): 75 NaCl, 28 Na<sub>2</sub>SO<sub>4</sub>, 3 KCl, 1.23 NaH<sub>2</sub>PO<sub>4</sub>, 1.48 MgCl<sub>2</sub>, 2 CaCl<sub>2</sub>, 26 NaHCO<sub>3</sub>, 10 glucose, and 10 mannitol, osmolality  $298 \pm 3\text{ mOsmol/kg}$ , 95% O<sub>2</sub>, 5% CO<sub>2</sub>. The  $+5\text{ mM}$  stimulus was achieved by brief bath application of the  $+15\text{ mM}$   $[\text{Na}^+]_o$  hypernatremic isosmotic ACSF that contained the following (in mM): 75 NaCl, 35 Na<sub>2</sub>SO<sub>4</sub>, 3 KCl, 1.23 NaH<sub>2</sub>PO<sub>4</sub>, 1.48 MgCl<sub>2</sub>, 2 CaCl<sub>2</sub>, 26 NaHCO<sub>3</sub>, and 10 glucose, osmolality  $298 \pm 3\text{ mOsmol/kg}$ , 95% O<sub>2</sub>, 5% CO<sub>2</sub>. In this case the internal solution was the same as that used in slice experiments.

For  $+36\text{ mM}$  stimulation the baseline solution contained the following (in mM): 136 NaCl, 3 KCl, 2 MgCl<sub>2</sub>, 2 CaCl<sub>2</sub>, and 10 HEPES,  $290 \pm 5\text{ mOsmol/kg}$ , pH 7.40. The  $+36\text{ mM}$   $[\text{Na}^+]$  hypernatremic-isosmotic solution contained the following (in mM): 46 Na<sub>3</sub>-citrate, 34 NaCl, 3 KCl, 2 MgCl<sub>2</sub>, 2 CaCl<sub>2</sub>, 10 HEPES, and 20 mannitol,  $290 \pm 5\text{ mOsmol/kg}$ , pH 7.40. The internal solution contained the following (in mM): 130 KCl, 10



$\text{NaCl}$ , 2  $\text{MgCl}_2$ , 0.02 EGTA, and 10 HEPES,  $290 \pm 5$  mOsmol/kg, pH 7.40 (all from Sigma-Aldrich).

**Immunohistochemistry.** Wistar rats were deeply anesthetized with 5% isoflurane and killed with a transcardiac perfusion of 4% paraformaldehyde (Sigma-Aldrich). Coronal brain sections of the SON (50  $\mu\text{m}$  thick) were cut using a VT-1200 vibratome. The sections were incubated for 1 h in blocking solution PBS containing 2% normal goat serum (NGS; Thermo Fisher Scientific) and 0.25% Triton X-100 (Sigma-Aldrich) at 4°C and then incubated overnight at 4°C using various primary antibodies (see above). The sections were washed in PBS containing 0.25% Triton X-100 and then incubated for 2 h at room temperature in PBS containing Alexa Fluor 647 anti-rabbit (1:500), Alexa Fluor 488 anti-guinea pig (1:500), Alexa Fluor 405 anti-mouse (1:500), and Alexa Fluor 568 anti-chicken (1:500; all from Invitrogen). All images were acquired using an FV3000 scanning laser confocal microscope (Olympus Canada). The analysis was performed with ImageJ software [National Institutes of Health (NIH)].

**AAV-mediated knockdown of  $\text{Na}_x$  channels in the MNCs of the SON.** Three adeno-associated viruses (AAVs) were used to induce shRNA knockdown of the  $\text{Na}_x$  channel (Vector Builds). The targeting sequences against rat *Scn7A* were the following: shRNA $_{\text{NaX1}}$  TAAGCAGGGAGGATCAAAATAT,  $1.66 \times 10^{13}$  GC/ml; shRNA $_{\text{NaX2}}$  GT AACACATCGTGTCTTTAAT,  $1.51 \times 10^{13}$  GC/ml; shRNA $_{\text{NaX3}}$  TGGC TCTGGAAGACATATATA,  $2.5 \times 10^{13}$  GC/ml. Expression was driven by the U6 promoter, which also induced expression of a mCherry reporter. To induce the specific knockdown of the  $\text{Na}_x$  channel in the SON, male Wistar rats GFP (12 weeks) were anesthetized with isoflurane 5% and stereotactically injected with 1  $\mu\text{l}$  of AAVs (mixture of the three shRNA $_{\text{NaX}(123)}$  or scRNA) in the SON (bregma,  $-1.1$ ; medio-lateral,  $\pm 1.8$ ; depth,  $-8.7$  mm). During the surgeries rats were kept anesthetized with 2.5% isoflurane and maintained at 37°C with a temperature controller (TCAT 2LV, Physitemp). Whole-cell recordings on slices were obtained 2–3 weeks postsurgery in the presence of TTX 0.5  $\mu\text{M}$ , benzamil 2  $\mu\text{M}$ , and SB-366791 3  $\mu\text{M}$ . The effectiveness of the knockdown was quantified by comparing the intensity of the anti- $\text{Na}_x$  signal in infected cells (relative to noninfected cells) in SON injected with AAVs driving shRNA $_{\text{NaX}}$  or scRNA.

**c-fos Analyses.** Rats were injected stereotactically in both SONs with AAVs (shRNA $_{\text{NaX}}$  in the right nucleus and scRNA in the left nucleus). After 2–3 weeks, these rats were injected with 2 M NaCl subcutaneously at a dose of 1.43 ml/kg or 3 M sucrose intraperitoneally at a dose of 1.91 ml/kg. One hour later the rats were anesthetized with isoflurane 5% and perfused with 4% paraformaldehyde (Sigma-Aldrich). Coronal brain sections of the SON (50  $\mu\text{m}$  thick) were cut using a VT1200 vibratome. The sections were blocked in PBS containing 10% NGS and 0.3% Triton X-100 for 1 h at 4°C. After washing with blocking solution, the sections were incubated with the anti-c-fos (1:2000) and anti-vasopressin (1:1000) primary antibodies overnight at 4°C. The sections were washed in PBS containing 0.3% Triton X-100 and then incubated for 2 h at room temperature in PBS containing Alexa Fluor 405 anti-rabbit (1:500) and Alexa Fluor 488 anti-guinea pig (1:500) secondary antibodies. All images were acquired using an FV3000 scanning laser confocal microscope (Olympus Canada). The analysis was performed with ImageJ software (NIH). For c-fos analyses we used an intensity threshold criterion to define positive and negative cells. The threshold used was determined by analyzing the distribution of intensities measured from >50 cells showing a clear positive signal, which showed zero overlap with the distribution of negative cells analyzed in the same sample. The numerical threshold was set at the value above which 95% of the positive cells were included. This approach slightly underestimated (~5%) the number of positive cells but avoided the inclusion of any false positive.

**Statistics.** All values in this study are reported as mean  $\pm$  SEM. Differences between groups were assessed using SigmaPlot 12.3 (Systat Software). The software first assessed normality of the data distribution and equal variance between groups. When these conditions were not met, a suitable nonparametric test was performed. All tests used for comparisons are specified in the text. Graphs were prepared using Prism 5.0 software (GraphPad), which was also used to calculate and plot linear regressions. In all statistical comparisons, differences were considered significant when  $p < 0.05$ .

## Results

### Female and male MNC<sup>OT</sup> and MNC<sup>VP</sup> respond equally to high $[\text{Na}^+]$

To determine whether identified MNC<sup>OT</sup> and MNC<sup>VP</sup> from females and males can respond to an increase in  $[\text{Na}^+]$  in the absence of an accompanying rise in osmolality, we performed experiments using acute hypothalamic slices prepared from adult double transgenic rats in which RFP and GFP are expressed in MNC<sup>OT</sup> and MNC<sup>VP</sup>, respectively (Ueta et al., 2005, 2008; Katoh et al., 2011; Fig. 1A,B). As illustrated in Figure 1, C and D, whole-cell voltage-clamp recordings ( $V_H = -50$  mV) showed that application of a ramp increase in  $[\text{Na}^+]_o$  delivered over 3 min under conditions where osmolality is unchanged, and peaking at +15 mM, evoked a gradual inward current in both types of neurons in females and males (see above, Materials and Methods). The mean peak increase in inward current was statistically significant in all cases (female MNC<sup>OT</sup>,  $-25.66 \pm 2.18$  pA,  $n = 10$  from 4 rats,  $p = 9.1 \times 10^{-7}$ ; female MNC<sup>VP</sup>,  $-23.11 \pm 2.42$  pA,  $n = 13$  from 6 rats,  $p = 5.9 \times 10^{-7}$ ; male MNC<sup>OT</sup>,  $-22.88 \pm 2.31$  pA,  $n = 14$  from 7 rats,  $p = 2.1 \times 10^{-7}$ ; male MNC<sup>VP</sup>,  $-25.26 \pm 3.79$  pA,  $n = 12$  from 5 rats,  $p = 3.5 \times 10^{-5}$ , all paired  $t$  tests), but was not statistically different between groups (one-way ANOVA,  $F = 0.263$ ,  $p = 0.851$ ; Fig. 1E).

In agreement with these findings, MNC<sup>OT</sup> and MNC<sup>VP</sup> from females and males were all progressively depolarized and excited by the same stimulus (Fig. 1C,D). The mean peak depolarization induced by  $\text{Na}^+$  was statistically significant (female MNC<sup>OT</sup>,  $3.6 \pm 0.5$  mV,  $n = 10$  from 4 rats,  $p = 2.9 \times 10^{-5}$ ; female MNC<sup>VP</sup>,  $4.7 \pm 1.2$  mV,  $n = 11$  from 7 rats,  $p = 2.4 \times 10^{-3}$ ; male MNC<sup>OT</sup>,  $4.8 \pm 1.1$  mV,  $n = 7$  from 4 rats,  $p = 5.7 \times 10^{-3}$ ; male MNC<sup>VP</sup>,  $4.0 \pm 0.7$  mV,  $n = 13$  from 7 rats,  $p = 7 \times 10^{-5}$ ; paired  $t$  tests) but was not statistically different between groups (one-way ANOVA,  $F = 0.414$ ,  $p = 0.744$ ; Fig. 1F). Similarly, the mean peak increase in action potential firing induced by  $\text{Na}^+$  was statistically significant (female MNC<sup>OT</sup>,  $5.5 \pm 1.57$  Hz,  $n = 9$  from 4 rats,  $p = 7.9 \times 10^{-3}$ ; female MNC<sup>VP</sup>,  $6.86 \pm 1.66$  Hz,  $n = 11$  from 6 rats,  $p = 2 \times 10^{-3}$ ; male MNC<sup>OT</sup>,  $7.12 \pm 1.57$  Hz,  $n = 7$  from 4 rats,  $p = 3.9 \times 10^{-3}$ ; male MNC<sup>VP</sup>,  $10.5 \pm 2.33$  Hz,  $n = 14$  from 7 rats,  $p = 5.8 \times 10^{-4}$ ; paired  $t$  tests) but was not statistically different between groups (one-way ANOVA,  $F = 1.28$ ,  $p = 0.295$ ; Fig. 1G). Instantaneous values of inward current measured as a function of bath  $[\text{Na}^+]_o$  were well correlated, allowing the  $\text{Na}^+$  sensitivity of each neuron to be quantified as the slope of a linear regression. As illustrated in Figure 1H, the  $\text{Na}^+$  sensitivity of MNC<sup>OT</sup> was equivalent to MNC<sup>VP</sup> and was also equivalent in females and males (one-way ANOVA,  $F = 1.485$ ,  $p = 0.231$ ).

To confirm the dose-dependent sensitivity to  $\text{Na}^+$  observed during ramps peaking at +15 mM, we also examined the effects of 3 min ramps peaking at lower concentrations. As shown in Figure 2, A and B, male MNC<sup>VP</sup> exposed to ramp  $\text{Na}^+$  stimuli between +3 and +15 mM  $[\text{Na}^+]_o$  displayed a statistically significant and dose-dependent peak inward current response to all stimuli (+3 mM,  $-1.07 \pm 0.30$  pA;  $n = 7$  from 5 rats,  $p = 0.0113$ ; +4 mM,  $-2.02 \pm 0.63$  pA;  $n = 8$  from 5 rats,  $p = 0.008$ ; +9 mM,  $-6.37 \pm 1.29$  pA;  $n = 8$  from 4 rats,  $p = 0.008$ ; paired  $t$  tests; Fig. 2C). Moreover, there was a linear relationship between the peak amplitude of the membrane current and the peak size of the  $\text{Na}^+$  stimulus. Notably the  $\text{Na}^+$  sensitivity assessed in this way (slope,  $-1.86$  pA/mM;  $r^2 = 0.72$ , different from zero,  $p < 0.0001$ ) was equivalent to that derived from the analyses in Figure 1H. Increases in peak ramp  $[\text{Na}^+]_o$  also caused significant and proportional peak

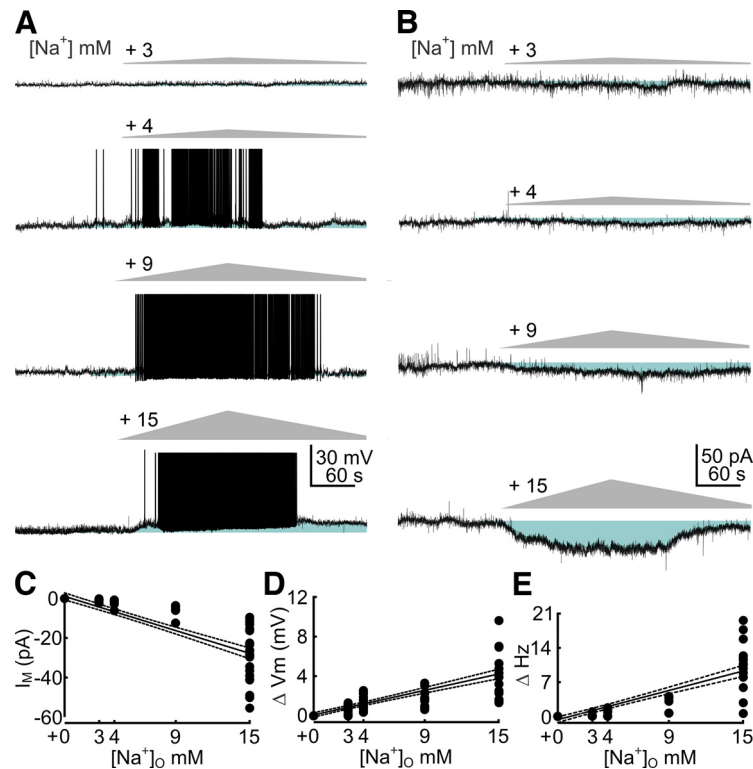


**Figure 2.** MNCs respond to a physiological  $[\text{Na}^+]$  challenge. **A**, Current-clamp recordings from  $\text{MNC}^{\text{VP}}$  in acute hypothalamic slices show effects of  $[\text{Na}^+]$  ramps (gray) with four different peak amplitudes (left of ramp). **B**, Voltage-clamp recordings from  $\text{MNC}^{\text{VP}}$  show effects of the same stimuli on membrane current ( $V_h = -50$  mV). **C**, Graph shows changes in membrane current ( $I_m$ ) induced by different peak  $[\text{Na}^+]$  stimuli. Each dot shows data from a different cell; the solid line is a linear regression fit, and the dashed line shows 95% confidence interval. **D**, Graph shows changes in membrane potential ( $\Delta V_m$ ) induced by different peak  $[\text{Na}^+]$  stimuli. Each dot shows data from a different cell; the solid line is a linear regression fit, and the dashed line shows 95% confidence interval. **E**, Graph shows changes in firing rate ( $\Delta \text{Hz}$ ) induced by different  $[\text{Na}^+]$  stimuli. Each dot shows data from a different cell; the solid line is a linear regression fit, and the dashed line shows 95% confidence interval.

changes in membrane potential (+3 mM,  $0.78 \pm 0.13$  mV;  $n = 11$  from 7 rats,  $p = 1.1 \times 10^{-4}$ ; +4 mM,  $1.31 \pm 0.18$  mV,  $n = 18$  from 8 rats,  $p = 1.6 \times 10^{-6}$ ; +9 mM,  $1.73 \pm 0.23$  mV;  $n = 12$  from 5 rats,  $p = 1.3 \times 10^{-5}$ ; paired  $t$  tests; Fig. 2D). There was also a linear relationship between the peak change in membrane potential and the peak ramp  $[\text{Na}^+]_o$  (slope,  $0.26$  mV/mM;  $r^2 = 0.65$ , different from zero,  $p < 0.0001$ ). Last, increases in peak ramp  $[\text{Na}^+]_o$  induced a proportional increase in peak action potential firing rate across the same range of stimuli (slope,  $0.59$  Hz/mM;  $r^2 = 0.59$ , different from zero,  $p < 0.0001$ ; Fig. 2E).

#### $\text{Na}_X$ is expressed in $\text{MNC}^{\text{OT}}$ and $\text{MNC}^{\text{VP}}$ but not in astrocytes

We examined the expression of  $\text{Na}_X$  in the SON using immunocytochemical staining with antibodies targeting VP, OT, GFAP, as well as an anti-Scn7A polyclonal antibody that targets an epitope on the distal portion of the cytoplasmic C terminus. No staining was observed when secondary antibodies were applied to sections not treated with these primary antibodies (Fig. 3A). The anti- $\text{Na}_X$  antibody revealed clear signals in areas expressing Scn7a (e.g., SON; Fig. 3B) but not in regions lacking this gene (e.g., red nucleus; Fig. 3C). As shown in Figure 3, D and E,  $\text{Na}_X$  was strongly expressed throughout the SON and was colocalized with both OT and VP. To determine whether  $\text{Na}_X$  is also expressed in astrocytes, we further stained the SON using an antibody directed against GFAP (glial fibrillary acidic protein). In contrast to MNC somata, we found that  $\text{Na}_X$  did not colocalize with GFAP (Fig. 3F,G). These results

suggest that  $\text{Na}_X$  may mediate responsiveness to  $\text{Na}^+$  in both  $\text{MNC}^{\text{OT}}$  and  $\text{MNC}^{\text{VP}}$ , and this property may not require the presence of  $\text{Na}_X$  in astrocytes.

To determine whether these neurons are intrinsically  $\text{Na}^+$  responsive, we examined the effect of hypernatremic-isosmotic stimuli on MNCs acutely isolated from the SON (Fig. 4A). As shown in Figure 4B, increasing  $[\text{Na}^+]_o$  by +5 mM caused a reversible membrane depolarization and increased firing under current clamp. These responses were proportional to peak stimulus intensity between 5 and 36 mM ( $n = 6$ ; data not shown). We then characterized the biophysical basis for these effects under voltage clamp. As shown in Figure 4, C and D, increasing  $[\text{Na}^+]_o$  by 36 mM caused a reversible inward membrane current ( $n = 4$  from 3 rats,  $p = 0.0156$ ; paired  $t$  test). To determine whether this inward current is mediated by  $\text{Na}^+$  influx, we obtained current-voltage relations in the absence and presence of high  $[\text{Na}^+]$ . As shown in Figure 4E,  $\text{Na}^+$  stimulation caused a significant increase in slope conductance (from  $0.39 \pm 0.07$  nS to  $0.83 \pm 0.10$  nS;  $p = 0.003$ , paired  $t$  test) and an  $E_{\text{Rev}}$  of  $17.5 \pm 2.5$  mV ( $n = 9$  from 4 rats; Fig. 4F,G), a value equivalent to  $E_{\text{Na}}$  under our conditions (19.9 mV;  $p = 0.3534$ , one-sample  $t$  test). Together these results indicate that MNCs respond to an increase in  $[\text{Na}^+]$  by the activation of  $\text{Na}^+$  selective ion channels.

#### $\text{Na}_X$ mediates $\text{Na}^+$ detection in MNCs *in vitro*

To determine whether channels other than  $\text{Na}_X$  contribute to the  $\text{Na}^+$ -activated current, we examined the effects of blockers of VGSCs (TTX,  $0.5$   $\mu\text{M}$ ;  $n = 10$ , 4 rats), Trpv1 (SB-366791,  $3$   $\mu\text{M}$ ;  $n = 11$ ; 4 rats), and ENaCs (benzamil,  $2$   $\mu\text{M}$ ;  $n = 9$ ; 5 rats). These

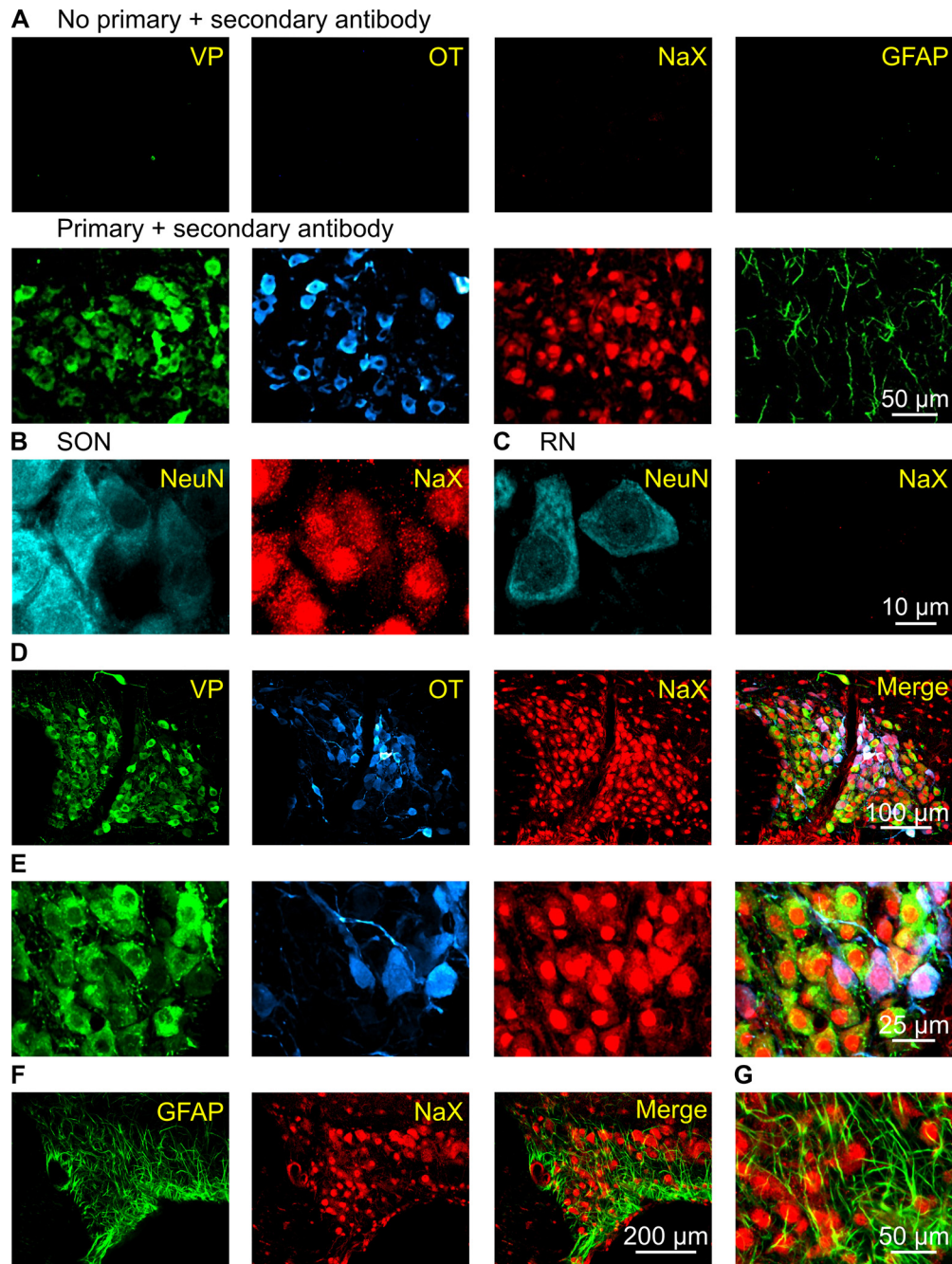


**Figure 3.**  $\text{Na}_x$  is expressed in  $\text{MNC}^{\text{OT}}$  and  $\text{MNC}^{\text{VP}}$  but not in astrocytes in rat SON. **A**, Confocal images show signals detected using our immunohistochemical procedure (bottom) were absent when stained in the absence of primary antibody (top). **B**, **C**, Specificity of the  $\text{Na}_x$  antibody is indicated by the presence of staining in SON neurons identified by the presence of NeuN (**B**) and absence of signal in NeuN-positive neurons of the red nucleus (RN; **C**), which does not express *Scn7A* according to the Allen Brain Atlas (<http://mouse.brain-map.org/gene/show/20035>). **D**, Confocal images show expression of VP (green), OT (blue),  $\text{Na}_x$  (red), and merged in a representative section through the SON. **E**, Higher-power views (layout the same as in **A**). **F**, Confocal images show expression of GFAP (green),  $\text{Na}_x$  (red), and merged. **G**, Higher-power view of the merged image in **F**.

blockers had no significant effect on the mean amplitude of the peak inward current induced by +15 mM  $\text{Na}^+$  ramp compared with control ( $n = 10$ ;  $p = 0.481$ ,  $H = 2.468$ , Kruskal–Wallis one-way ANOVA on ranks; Fig. 5A,B).

Because there are no selective blockers of  $\text{Na}_x$  channels, we used a viral vector strategy to selectively reduce the expression of these channels *in vivo* before testing their activity *in vitro*. As illustrated in Figure 6A, AAVs driving the expression of an anti-*Scn7a* shRNA (shRNA $_{\text{Na}_x}$ ), or a scramble control (scRNA), were stereotactically injected separately into each SON. Both AAV constructs also induced expression of mCherry as a reporter

(Fig. 6B), allowing identification of infected cells in acute brain slices prepared 2–3 weeks after injection (Fig. 6C). The average intensity of the mCherry signal was equivalent in neurons infected by shRNA $_{\text{Na}_x}$  ( $n = 106$ , 3 rats) and scRNA ( $n = 130$ , 3 rats;  $p = 0.7847$ , Mann–Whitney test). Quantification of anti- $\text{Na}_x$  immunofluorescence revealed that AAV infection reduced  $\text{Na}_x$  expression in both groups but that  $\text{Na}_x$  expression was 36% lower in shRNA $_{\text{Na}_x}$  than scRNA  $p < 0.0001$ , Mann–Whitney rank sum test; Figure 6D,E). To isolate the current induced by  $\text{Na}_x$  as much as possible, these experiments were performed in the presence of TTX, SB-366971, and Benzamil (same concentrations as above).



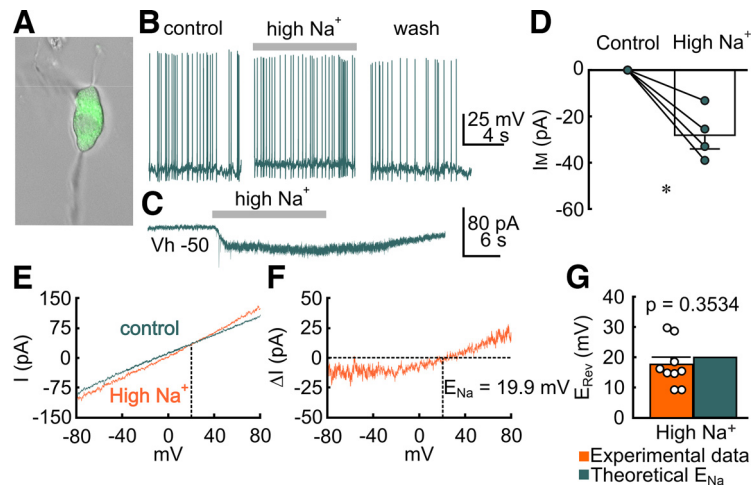


**Figure 4.** Effects of high  $\text{Na}^+$  in isolated MNCs. **A**, Image of an isolated MNC<sup>VP</sup> (GFP in green). **B**, Traces show effects in increasing  $\text{Na}^+$  by +5 mM under current clamp. **C**, Trace shows effects in increasing  $\text{Na}^+$  by +36 mM on membrane current ( $I_m$ ) recorded under voltage clamp (left,  $V_h$ ). **D**, Bar graph shows mean  $\pm$  SEM changes in  $I_m$  induced by high  $\text{Na}^+$ . Each line joins data points from a different cell; \* $p = 0.0156$ , paired  $t$  test. **E**,  $I$ - $V$  plot ( $V_h$ ,  $-40$  mV; ramp,  $-80$  to  $+80$  mV, 1.5 s) recorded from a MNC in the absence (control, teal) and presence (orange) of high  $\text{Na}^+$ . Dotted line shows approximate  $E_{\text{Na}}$ . **F**, Difference current ( $\Delta I$ )  $I$ - $V$  plot obtained by subtraction of traces in **E**. **G**, Orange bar shows the mean  $\pm$  SEM  $E_{\text{Rev}}$  of the current induced by high  $\text{Na}^+$  (each dot is data from a different cell). Teal bar shows theoretical  $E_{\text{Na}}$  in these conditions.

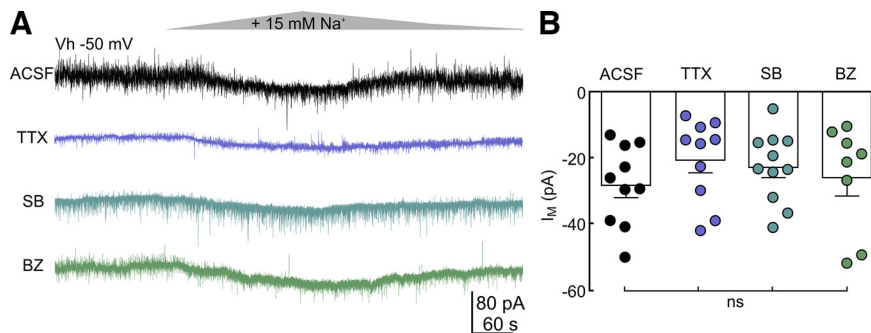


**Figure 5.** The current induced by high  $\text{Na}^+$  is not affected by blocking VGSCs, Trpv1, or ENaCs. **A**, Voltage-clamp recordings ( $V_h$ ,  $-50$  mV) show the inward current induced by high  $\text{Na}^+$  is not blocked by TTX ( $0.5 \mu\text{M}$ ; purple trace), the Trpv1 blocker SB-366791 ( $3 \mu\text{M}$ ; blue trace), and the ENaC blocker benzamil (BZ;  $2 \mu\text{M}$ ; green trace). **B**, Bar graph shows mean and  $\pm$  SEM peak amplitudes of the inward current ( $I_m$ ) recorded in the absence (ACSF) or presence of different blockers. Each dot is the response of one MNC. ns, Not significant.

As illustrated in Figure 6, *F* and *G*, the peak current induced by a +15 mM  $\text{Na}^+$  ramp was significantly smaller in cells infected with shRNA<sub>NaX</sub> ( $-4.30 \pm 1.92$  pA,  $n = 12$  from 3 rats) compared with cells infected with scRNA ( $-18.38 \pm 2.70$  pA,  $n = 13$  from 4 rats), adjacent uninfected cells ( $-27.24 \pm 5.16$  pA,  $n = 4$  from 3 rats), and control MNC<sup>VP</sup> in slices prepared from uninjected animals ( $-28.36 \pm 3.84$  pA,  $n = 10$  from 6 rats;  $p < 0.001$ ,  $H = 21.113$ , Kruskal–Wallis one-way ANOVA on ranks and Dunn's *post hoc* test).

#### **$\text{Na}_X$ expression in MNCs contributes to detection of changes in $[\text{Na}^+]_o$ but not osmolality *in vivo***

The data reported above indicate that  $\text{Na}_X$  channels allow MNCs to detect increases in  $[\text{Na}^+]_o$  independently of osmotic changes *in vitro*. To determine whether  $\text{Na}_X$  channels contribute to  $\text{Na}^+$  detection but not osmotic detection *in vivo*, we compared the degree of *c-fos* induction caused by injection of 2 M NaCl (1.43 ml/kg, s.c.) or 3 M sucrose (1.91 ml/kg, i.p.) in MNCs expressing shRNA<sub>NaX</sub> or scRNA (Fig. 7*A*). In these experiments each animal was injected with shRNA<sub>NaX</sub> in one SON and scRNA in the other SON. Two to 3 weeks after this procedure the rats were injected with 2 M NaCl or 3 M sucrose and perfused with paraformaldehyde 60 min later. As illustrated in Figure 7, *B* and *C*, injection of

2 M NaCl caused a significant increase in both serum  $[\text{Na}^+]$  ( $p = 0.006$ , Mann–Whitney rank sum test,  $t$  test) and osmolality ( $p = 0.025$ ,  $t$  test), whereas injection of 3 M sucrose caused an equivalent increase in osmolality ( $p = 0.019$ , Mann–Whitney rank sum test,  $t$  test) without affecting serum  $[\text{Na}^+]$  ( $p = 0.715$ ,  $t$  test). Interestingly, the proportion of infected MNCs expressing *c-fos* following 3 M sucrose injection was not affected by  $\text{Na}_X$  knockdown (shRNA<sub>NaX</sub>,  $20.07 \pm 1.66\%$ ,  $n = 7$ ; scRNA,  $19.99 \pm 1.74\%$ ,  $n = 3$ ;  $p = 0.489$ ,  $t$  test). However,  $\text{Na}_X$  knockdown significantly reduced the proportion of infected MNCs expressing *c-fos* following 2 M NaCl injection (shRNA<sub>NaX</sub>,  $9.95 \pm 0.66\%$ ;  $n = 6$ ; scRNA,  $20.72 \pm 2.94\%$ ;  $n = 4$ ,  $p = 0.002$ ,  $t$  test). Together, these results indicate that  $\text{Na}_X$  contributes to  $\text{Na}^+$  detection but not osmosensitivity by MNCs.

#### **Discussion**

Combinations of anatomic, chemo/optogenetic, lesion, and genetic studies have established that both osmoreceptors and  $\text{Na}^+$  detectors located in the SFO and OVLT mediate feedback control of osmoregulatory responses (Denton et al., 1996; McKinley and Johnson, 2004; Noda and Hiyama, 2015; Zimmerman et al., 2017; Gizowski and Bourque, 2018). In agreement, electrophysiological experiments have shown

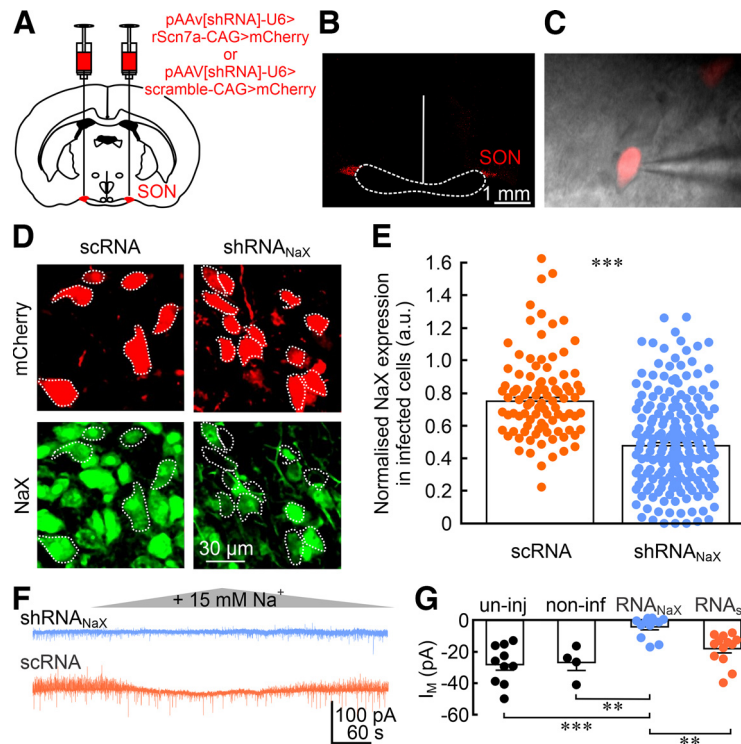


**Figure 6.** Reducing the expression of  $\text{Scn7a}$  impairs the inward current response to high  $\text{Na}^+$ . **A**, AAVs driving expression of shRNA $_{\text{NaX}}$  or scRNA (and mCherry reporter) were injected in the SON bilaterally (1  $\mu\text{l}$ ). **B**, Three weeks later brain slices were prepared for electrophysiology, and AAV-driven mCherry expression was visible (Dashed line represents optic chiasm.). **C**, Patch-clamp recordings were obtained from cells expressing mCherry. **D**, Infected cells expressing mCherry (top) and corresponding immunoreactivity against  $\text{Na}_X$  (bottom) in SON injected with scRNA and shRNA $_{\text{NaX}}$ . Dotted lines indicate selected cells. **E**, Bar graphs show mean  $\pm$  SEM values of the intensity of the anti- $\text{Na}_X$  signal in infected cells calculated as a ratio of intensity divided by the average intensity of the  $\text{Na}_X$  signal measured in noninfected cells in the same section; \*\*\* $p$  < 0.001. Each point is data for a different cell. **F**, Traces show examples of membrane current responses ( $V_{\text{h}}$ ,  $-50$  mV) to high  $\text{Na}^+$  recorded from cells infected with shRNA $_{\text{NaX}}$  (blue) and scRNA (orange). **G**, Bar graphs show mean  $\pm$  SEM peak amplitudes of the membrane current ( $I_{\text{M}}$ ) responses to high  $\text{Na}^+$  in MNCs from uninjected (un-inj) animals, noninfected cells (non-inf), and MNCs infected with shRNA $_{\text{NaX}}$  (RNA $_{\text{NaX}}$ ) and scRNA (RNA $_{\text{sc}}$ ); \*\* $p$  < 0.01, \*\*\* $p$  < 0.001.

that the action potential firing rate of neurons in the SFO and OVLT can be affected by changes in extracellular fluid osmolality (Sayer et al., 1984; Sibbald et al., 1988; Anderson et al., 2000; Ciura and Bourque, 2006; Ciura et al., 2011) or  $[\text{Na}^+]$  (Vivas et al., 1990; Anderson et al., 2000; Hiyama et al., 2002; Ciura and Bourque, 2006; Ciura et al., 2011) and regulate the firing of downstream osmoregulatory effector neurons via synaptic effects (Richard and Bourque, 1995; Trudel and Bourque, 2010; Kim et al., 2021). Interestingly, osmoregulatory effector neurons such as MNC $^{\text{VP}}$  and MNC $^{\text{OT}}$  also express intrinsic osmo- and  $\text{Na}^+$ -sensing properties (Mason, 1980; Olet and Bourque, 1994; Voisin et al., 1999; Zaelzer et al., 2015). However, the effects of selectively ablating such properties in MNCs had never been examined, and thus it remained unclear if such properties contribute or not to the regulation of these neurons under physiological conditions. Our *in vitro* experiments reveal that  $\text{Na}_X$  channels expressed in MNC $^{\text{VP}}$  and MNC $^{\text{OT}}$  allow these neurons to become depolarized and excited when exposed to a physiologically relevant increase in  $[\text{Na}^+]_{\text{o}}$  ( $\sim 4$  mM) that occurs in the absence of an accompanying osmotic challenge. Moreover, *in vivo* experiments showed that  $\text{Na}_X$  expression within MNCs contributes significantly to the activation of these neurons in response to an equivalent increase in serum  $[\text{Na}^+]$ . Together, these findings indicate that MNCs can act as intrinsic  $\text{Na}^+$  detectors, and this property contributes significantly to the activation of these neurons under hypernatremic conditions.

Previous studies have suggested that many types of ion channels could potentially mediate  $\text{Na}^+$  detection in MNCs. Notably, the density of slowly inactivating VGSCs is enhanced by chronic

salt loading (Waxman et al., 2000). However, our data indicate that the inward current induced by an acute  $\text{Na}^+$  stimulus is unaffected by TTX, which blocks most VGSCs. Although the TTX-insensitive  $\text{Na}^+$  channel Nav1.9 is expressed in MNCs (Black et al., 2014) and appears to be fully inactivated at voltages near the resting potential of MNCs, it has been suggested that a small steady-state window current may exist because of overlap of activation and inactivation curves in this range. If this is the case, it is conceivable that Nav1.9 could make a small contribution to  $\text{Na}^+$  detection. Additional experiments are required to examine whether TTX-insensitive VGSCs contribute to the non- $\text{Na}_X$  current induced by increased  $[\text{Na}^+]_{\text{o}}$ . Previous experiments have shown that the density of ENaCs in the membrane of MNCs is increased by prolonged high salt intake and contributes to membrane depolarization under those conditions (Sharma et al., 2017). However, our data show that responses to acute high  $[\text{Na}^+]$  stimuli are unaffected by the selective ENaC blocker benzamil. Therefore, ENaCs do not appear to mediate  $\text{Na}^+$  detection by MNCs during acute perturbations in euhydrated animals.

A previous study from our laboratory showed that  $\text{Na}^+$  stimuli can depolarize isolated MNCs by increasing the leak current flowing through stretch-inhibited cation channels, and this effect was potentiated when cells were shrunk by hypertonicity (Voisin et al., 1999). Later studies have identified this channel as an N-terminal variant of Trpv1 ( $\Delta\text{N-Trpv1}$ ; Sharif-Naeini et al., 2006; Zaelzer et al., 2015) that can be blocked by SB-366791 (Sharif-Naeini et al., 2008; Ciura et al., 2011). Our present experiments showed that SB-366791 does not significantly reduce responses induced by  $\text{Na}^+$  stimuli delivered on MNCs in slices



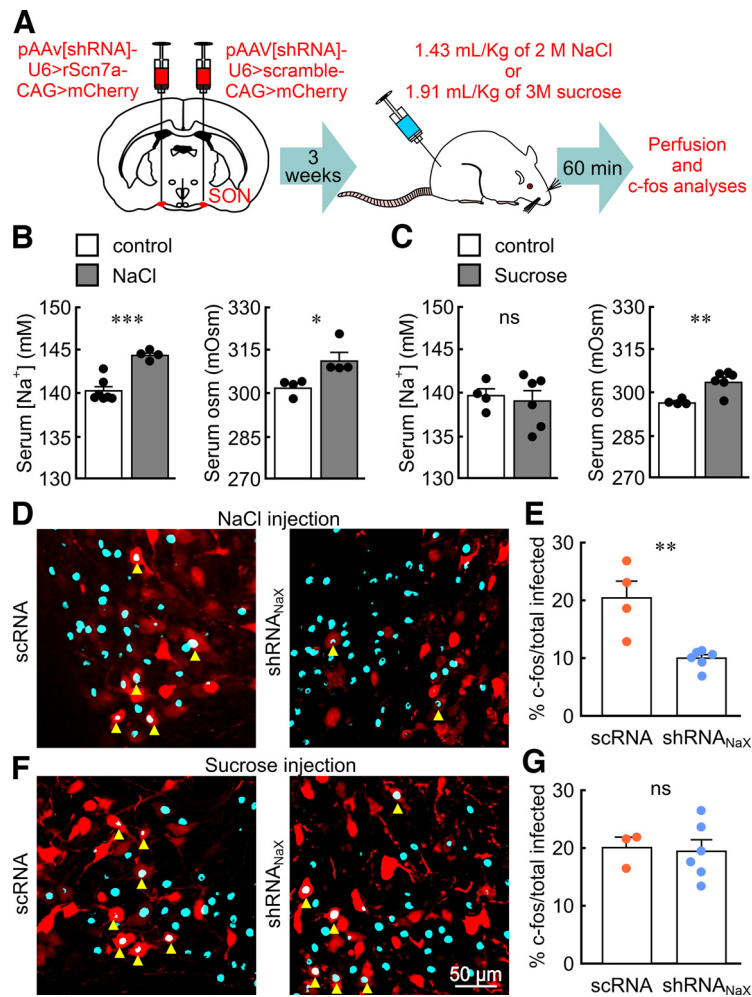


**Figure 7.** Downregulating *Scn7a* in MNCs impairs the response to systemic high  $\text{Na}^+$  *in vivo*. **A**, AAVs driving expression of shRNA $_{\text{NaX}}$  and scRNA (and mCherry reporter) were respectively injected in the right and left SONs of each animal (1  $\mu\text{L}$ ). Three weeks later, animals were injected subcutaneously with NaCl (2 M) or intraperitoneally with sucrose (3 M) and prepared for *c-fos* analyses. **B**, Bar graphs show mean  $\pm$  SEM values of serum  $[\text{Na}^+]$  (left) and serum osmolality (right) observed 20 min after injection of NaCl. **C**, Bar graphs show mean  $\pm$  SEM values of serum  $[\text{Na}^+]$  (left) and serum osmolality (right) observed 20 min after injection of sucrose; \*\* $p < 0.01$ , ns, Not significant; \* $p < 0.1$ , \*\*\* $p < 0.001$ . **D**, Images show that NaCl is less effective at inducing *c-fos* in cells transduced with shRNA $_{\text{NaX}}$ . Yellow arrows indicate infected cells expressing *c-fos*. **E**, Bar graphs show mean  $\pm$  SEM fraction of cells expressing *c-fos* in MNCs infected with shRNA $_{\text{NaX}}$  and scRNA in NaCl-injected rats; \*\* $p < 0.01$ . **F**, Images show that sucrose is equally effective at inducing *c-fos* in cells infected with shRNA $_{\text{NaX}}$  or scRNA. **G**, Bar graphs show mean  $\pm$  SEM fraction of cells expressing *c-fos* in MNCs infected with shRNA $_{\text{NaX}}$  and scRNA in sucrose-injected rats (each dot shows data from a different animal).

maintained under isotonic conditions. Therefore,  $\Delta\text{N-Trpv1}$  channels do not appear to mediate  $\text{Na}^+$  detection by MNCs during acute perturbations in euhydrated animals. Whether  $\Delta\text{N-Trpv1}$ , ENaC, and/or VGSCs contribute to  $\text{Na}^+$  detection under other conditions (e.g., dehydration) remains to be determined.

Previous work has shown that  $\text{Na}_x$  is expressed in glial cells in the SFO (Shimizu et al., 2007) and OVLT (Nomura et al., 2019), and that the excitatory effects of high  $[\text{Na}^+]$  on neurons in these nuclei are mediated indirectly by the  $\text{Na}_x$ -dependent release of lactate,  $\text{H}^+$ , and other signaling cascades (Noda and Hiyama, 2015). However, in agreement with a previous study (Nehmé et al., 2012), our experiments indicate that in the SON the  $\text{Na}_x$  channel is expressed in MNCs but not astrocytes. This suggests that the mechanism by which  $\text{Na}_x$  depolarizes neurons in the SON may be different from in the SFO and OVLT. In principle, the inward current induced by increased extracellular  $[\text{Na}^+]$  could simply reflect the associated increase in driving force. Indeed, *I-V* curves recorded in the presence and absence of high  $\text{Na}^+$  were parallel to each other at negative voltages (Fig. 4E), as observed previously (Voisin et al., 1999). However, we also observed that a high  $\text{Na}^+$  stimulus caused an increase in

membrane  $\text{Na}^+$  conductance at positive voltages, giving the  $\text{Na}^+$ -induced current a strong degree of outward rectification (Fig. 4F). This result suggests that the inward current induced in MNCs involves an increase in the activity of  $\text{Na}_x$  channels. Interestingly,  $\text{Na}_x$  channels expressed alone in recombinant systems fail to conduct ions (Noland et al., 2022), suggesting that interactions with accessory subunits and proteins such as the NaK-ATPase are required to form functional  $\text{Na}^+$  sensor channels *in situ* (Berret et al., 2013; Noda and Hiyama, 2015). Additional experiments are required to establish the molecular mechanism underlying  $\text{Na}_x$  activation in MNCs, as well as the basis for outward rectification. Our conclusion that  $\text{Na}^+$  detection by MNCs requires  $\text{Na}_x$  channels is based on the observation that selectively decreasing their expression with an *Scn7a*-specific shRNA significantly reduced the inward current induced by  $\text{Na}^+$  stimulation *in vitro* and neuronal activation in response to  $[\text{Na}^+]_o$  elevation *in vivo*. Although immunochemical analyses suggested that the shRNA approach only reduced  $\text{Na}_x$  expression by 36% compared with scRNA, we observed a 76.6% reduction in peak  $\text{Na}^+$ -induced current measured by whole-cell recording. This observation suggests that our immunochemical

approach underestimated the degree of Na<sub>x</sub> expression or that expression and channel function are not linearly related. Interestingly, a previous study has shown that expression of *Scn7A* is increased in response to dehydration (Pauz̃a et al., 2021), suggesting that Na<sub>x</sub> channels may contribute significantly more to Na<sup>+</sup> detection in this condition.

Under most physiological conditions, increases in osmolality associated with fluid loss (e.g., dehydration) are accompanied by proportional changes in extracellular [Na<sup>+</sup>], such that both of these parameters vary in concert. Why separate mechanisms exist for detection of Na<sup>+</sup> and osmolality is unclear. However, it is important to consider that these variables can become dissociated from one another under pathologic states (Iwasaki et al., 1996; Ahloulay et al., 1999). For example, hyperglycemia associated with diabetes mellitus is a condition in which hyponatremia can occur in the absence of hypoosmolality (Liamis et al., 2014). As such, the existence of distinct osmo- and Na<sup>+</sup>-sensing mechanisms allows MNCs to monitor these parameters separately, which may confer simple redundancy or impart functional aspects that remain to be established.

## References

- Abe H, Ogata N (1982) Ionic mechanism for the osmotically-induced depolarization in neurones of the guinea-pig supraoptic nucleus *in vitro*. *J Physiol* 327:157–171.
- Ahloulay M, Schmitt F, Dechaux M, Bankir L (1999) Vasopressin and urinary concentrating activity in diabetes mellitus. *Diabetes Metab* 25:213–222.
- Anderson JW, Washburn DL, Ferguson AV (2000) Intrinsic osmosensitivity of subfornical organ neurons. *Neuroscience* 100:539–547.
- Andersson B (1977) Regulation of body fluids. *Annu Rev Physiol* 39:185–200.
- Augustine V, Gokce SK, Lee S, Wang B, Davidson TJ, Reimann F, Gribble F, Deisseroth K, Lois C, Oka Y (2018) Hierarchical neural architecture underlying thirst regulation. *Nature* 555:204–209.
- Berret E, Nehmé B, Henry M, Toth K, Drolet G, Mouginit D (2013) Regulation of central Na<sup>+</sup> detection requires the cooperative action of the NaX channel and  $\alpha$ 1 isoform of Na<sup>+</sup>/K<sup>+</sup>-ATPase in the Na<sup>+</sup>-sensor neuronal population. *J Neurosci* 33:3067–3078.
- Black JA, Vasylyev D, Dib-Hajj SD, Waxman SG (2014) Nav1.9 expression in magnocellular neurosecretory cells of supraoptic nucleus. *Exp Neurol* 253:174–179.
- Bourque CW (2008) Central mechanisms of osmosensation and systemic osmoregulation. *Nat Rev Neurosci* 9:519–531.
- Ciura S, Bourque CW (2006) Transient receptor potential vanilloid 1 is required for intrinsic osmoreception in organum vasculosum lamina terminalis neurons and for normal thirst responses to systemic hyperosmolality. *J Neurosci* 26:9069–9075.
- Ciura S, Liedtke W, Bourque CW (2011) Hypertonicity sensing in organum vasculosum lamina terminalis neurons: a mechanical process involving TRPV1 but not TRPV4. *J Neurosci* 31:14669–14676.
- Ciura S, Prager-Khoutorsky M, Thirouin ZS, Wyrosdick JC, Olson JE, Liedtke W, Bourque CW (2018) Trpv4 mediates hypotonic inhibition of central osmosensory neurons via taurine gliotransmission. *Cell Rep* 23:2245–2253.
- Denton DA, McKinley MJ, Weisinger RS (1996) Hypothalamic integration of body fluid regulation. *Proc Natl Acad Sci U S A* 93:7397–7404.
- Gizowski C, Bourque CW (2018) The neural basis of homeostatic and anticipatory thirst. *Nat Rev Nephrol* 14:11–25.
- Hiyama TY, Watanabe E, Ono K, Inenaga K, Tamkun MM, Yoshida S, Noda M (2002) Na(x) channel involved in CNS sodium-level sensing. *Nat Neurosci* 5:511–512.
- Hiyama TY, Watanabe E, Okado H, Noda M (2004) The subfornical organ is the primary locus of sodium-level sensing by Na(x) subdomain channels for the control of salt-intake behavior. *J Neurosci* 24:9276–9281.
- Hiyama TY, Matsuda S, Fujikawa A, Matsumoto M, Watanabe E, Kajiwar H, Niimura F, Noda M (2010) Autoimmunity to the sodium-level sensor in the brain causes essential hypernatremia. *Neuron* 66:508–522.
- Huang W, Lee SL, Sjöquist M (1995) Natriuretic role of endogenous oxytocin in male rats infused with hypertonic NaCl. *Am J Physiol* 268:R634–640.
- Iwasaki Y, Kondo K, Murase T, Hasegawa H, Oiso Y (1996) Osmoregulation of plasma vasopressin in diabetes mellitus with sustained hyperglycemia. *J Neuroendocrinol* 8:755–760.
- Katoh A, Fujihara H, Ohbuchi T, Onaka T, Hashimoto T, Kawata M, Suzuki H, Ueta Y (2011) Highly visible expression of an oxytocin-monomeric red fluorescent protein 1 fusion gene in the hypothalamus and posterior pituitary of transgenic rats. *Endocrinology* 152:2768–2774.
- Kim A, Madara JC, Wu C, Andermann ML, Lowell BB (2021) Neural basis for regulation of vasopressin secretion by anticipated disturbances in osmolality. *Elife* 10:e66609.
- Liamis G, Liberopoulos E, Barkas F, Elisaf M (2014) Diabetes mellitus and electrolyte disorders. *World J Clin Cases* 2:488–496.
- Mandelblat-Cerf Y, Kim A, Burgess CR, Subramanian S, Tannous BA, Lowell BB, Andermann ML (2017) Bidirectional anticipation of future osmotic challenges by vasopressin neurons. *Neuron* 93:57–65.
- Mason WT (1980) Supraoptic neurones of rat hypothalamus are osmosensitive. *Nature* 287:154–157.
- McKinley MJ, Johnson AK (2004) The physiological regulation of thirst and fluid intake. *News Physiol Sci* 19:1–6.
- McKinley MJ, Denton DA, Weisinger RS (1978) Sensors for antidiuresis and thirst—osmoreceptors or CSF sodium detectors? *Brain Res* 141:89–103.
- Nehmé B, Henry M, Mouginit D, Drolet G (2012) The expression pattern of the Na(+) sensor, Na(X) in the hydromineral homeostatic network: a comparative study between the rat and mouse. *Front Neuroanat* 6:26.
- Noda M, Hiyama TY (2015) Sodium sensing in the brain. *Pflugers Arch* 467:465–474.
- Noda M, Matsuda T (2022) Central regulation of body fluid homeostasis. *Proc Jpn Acad Ser B Phys Biol Sci* 98:283–324.
- Noland CL, Chua HC, Kschonsak M, Heusser SA, Braun N, Chang T, Tam C, Tang J, Arthur CP, Ciferri C, Pless SA, Payandeh J (2022) Structure-guided unlocking of NaX reveals a non-selective tetrodotoxin-sensitive cation channel. *Nat Commun* 13:1416.
- Nomura K, Hiyama TY, Sakuta H, Matsuda T, Lin CH, Kobayashi K, Kobayashi K, Kuwaki T, Takahashi K, Matsui S, Noda M (2019) [Na<sup>+</sup>] increases in body fluids sensed by central Na(x) induce sympathetically mediated blood pressure elevations via H<sup>+</sup>-dependent activation of ASIC1a. *Neuron* 101:60–75.e6.
- Oka Y, Ye M, Zuker CS (2015) Thirst driving and suppressing signals encoded by distinct neural populations in the brain. *Nature* 520:349–352.
- Oliet SH, Bourque CW (1992) Properties of supraoptic magnocellular neurones isolated from the adult rat. *J Physiol* 455:291–306.
- Oliet SH, Bourque CW (1993) Mechanosensitive channels transduce osmosensitivity in supraoptic neurons. *Nature* 364:341–343.
- Oliet SH, Bourque CW (1994) Osmoreception in magnocellular neurosecretory cells: from single channels to secretion. *Trends Neurosci* 17:340–344.
- Olsson K, Kolmodin R (1974) Dependence of basic secretion of antidiuretic hormone on cerebrospinal fluid (Na<sup>+</sup>). *Acta Physiol Scand* 91:286–288.
- Pauz̃a AG, Mecawi AS, Paterson A, Hindmarch CCT, Greenwood M, Murphy D, Greenwood MP (2021) Osmoregulation of the transcriptome of the hypothalamic supraoptic nucleus: a resource for the community. *J Neuroendocrinol* 33:e13007.
- Pool AH, Wang T, Stafford DA, Chance RK, Lee S, Ngai J, Oka Y (2020) The cellular basis of distinct thirst modalities. *Nature* 588:112–117.
- Prager-Khoutorsky M, Khoutorsky A, Bourque CW (2014) Unique interwoven microtubule scaffold mediates osmosensory transduction via physical interaction with TRPV1. *Neuron* 83:866–878.
- Richard D, Bourque CW (1995) Synaptic control of rat supraoptic neurones during osmotic stimulation of the organum vasculosum lamina terminalis *in vitro*. *J Physiol* 489 (Pt 2):567–577.
- Robertson GL, Shelton RL, Athar S (1976) The osmoregulation of vasopressin. *Kidney Int* 10:25–37.
- Sayer RJ, Hubbard JJ, Sirett NE (1984) Rat organum vasculosum laminae terminalis *in vitro*: responses to transmitters. *Am J Physiol* 247:R374–379.
- Sharif-Naeini R, Witty MF, Séguéla P, Bourque CW (2006) An N-terminal variant of Trpv1 channel is required for osmosensory transduction. *Nat Neurosci* 9:93–98.
- Sharif-Naeini R, Ciura S, Bourque CW (2008) TRPV1 gene required for thermosensory transduction and anticipatory secretion from vasopressin neurons during hyperthermia. *Neuron* 58:179–185.

- Sharma K, Haque M, Guidry R, Ueta Y, Teruyama R (2017) Effect of dietary salt intake on epithelial  $\text{Na}^+$  channels (ENaC) in vasopressin magnocellular neurosecretory neurons in the rat supraoptic nucleus. *J Physiol* 595:5857–5874.
- Shimizu H, Watanabe E, Hiyama TY, Nagakura A, Fujikawa A, Okado H, Yanagawa Y, Obata K, Noda M (2007) Glial  $\text{Na}^+$  channels control lactate signaling to neurons for brain  $[\text{Na}^+]$  sensing. *Neuron* 54:59–72.
- Sibbald JR, Hubbard JI, Sirett NE (1988) Responses from osmosensitive neurons of the rat subfornical organ *in vitro*. *Brain Res* 461:205–214.
- Stachniak TJ, Trudel E, Bourque CW (2014) Cell-specific retrograde signals mediate antiparallel effects of angiotensin II on osmoreceptor afferents to vasopressin and oxytocin neurons. *Cell Rep* 24:355–362.
- Teruyama R, Sakuraba M, Wilson LL, Wandrey NE, Armstrong WE (2012) Epithelial  $\text{Na}^+$  sodium channels in magnocellular cells of the rat supraoptic and paraventricular nuclei. *Am J Physiol Endocrinol Metab* 302:E273–E285.
- Trudel E, Bourque CW (2010) Central clock excites vasopressin neurons by waking osmosensory afferents during late sleep. *Nat Neurosci* 13:467–474.
- Ueta Y, Fujihara H, Serino R, Dayanithi G, Ozawa H, Matsuda K, Kawata M, Yamada J, Ueno S, Fukuda A, Murphy D (2005) Transgenic expression of enhanced green fluorescent protein enables direct visualization for physiological studies of vasopressin neurons and isolated nerve terminals of the rat. *Endocrinology* 146:406–413.
- Ueta Y, Fujihara H, Dayanithi G, Kawata M, Murphy D (2008) Specific expression of optically active reporter gene in arginine vasopressin-secreting neurosecretory cells in the hypothalamic-neurohypophyseal system. *J Neuroendocrinol* 20:660–664.
- Vivas L, Chiaraviglio E, Carrer HF (1990) Rat organum vasculosum laminae terminalis *in vitro*: responses to changes in sodium concentration. *Brain Res* 519:294–300.
- Voisin DL, Bourque CW (2002) Integration of sodium and osmosensory signals in vasopressin neurons. *Trends Neurosci* 25:199–205.
- Voisin DL, Chakfe Y, Bourque CW (1999) Coincident detection of CSF  $\text{Na}^+$  and osmotic pressure in osmoregulatory neurons of the supraoptic nucleus. *Neuron* 24:453–460.
- Waxman SG, Dib-Hajj S, Cummins TR, Black JA (2000) Sodium channels and their genes: dynamic expression in the normal nervous system, dysregulation in disease states(1). *Brain Res* 886:5–14.
- Zaelzer C, Hua P, Prager-Khoutorsky M, Ciura S, Voisin DL, Liedtke W, Bourque CW (2015)  $\Delta\text{N-TRPV1}$ : a molecular co-detector of body temperature and osmotic stress. *Cell Rep* 13:23–30.
- Zimmerman CA, Leib DE, Knight ZA (2017) Neural circuits underlying thirst and fluid homeostasis. *Nat Rev Neurosci* 18:459–469.
- Zimmerman CA, Huey EL, Ahn JS, Beutler LR, Tan CL, Kosar S, Bai L, Chen Y, Corpuz TV, Madisen L, Zeng H, Knight ZA (2019) A gut-to-brain signal of fluid osmolarity controls thirst satiation. *Nature* 568:98–102.